Available online at www.sciencedirect.com

ScienceDirect

journal homepage: www.elsevier.com/locate/issn/15375110

Research Paper

Integration of simultaneous tactile sensing and visible and near-infrared reflectance spectroscopy in a robot gripper for mango quality assessment

Victoria Cortés [a], Carlos Blanes [b], José Blasco [c], Coral Ortíz [d], Nuria Aleixos [e], Martín Mellado [b], Sergio Cubero [c], Pau Talens [a,*]

[a] Departamento de Tecnología de Alimentos, Universitat Politècnica de València, Camino de Vera, s/n, 46022 Valencia, Spain

[b] Instituto de Automática e Informática Industrial, Universitat Politècnica de València, Camino de Vera s/n, 46022 Valencia, Spain

[c] Centro de Agroingeniería, Instituto Valenciano de Investigaciones Agrarias (IVIA), Ctra. Moncada-Náquera Km 4.5, 46113, Moncada, Valencia, Spain

[d] Departamento de Ingeniería Rural y Agroalimentaria, Universitat Politècnica de València, Camino de Vera s/n, 46022 Valencia, Spain

[e] Departamento de Ingeniería Gráfica, Universitat Politècnica de València, Camino de Vera, s/n, 46022 Valencia, Spain

ARTICLE INFO

Article history:
Received 18 April 2017
Received in revised form
18 June 2017
Accepted 6 August 2017
Published online 30 August 2017

Keywords:
Spectrometry
Chemometrics
Non-destructive sensor
Tactile sensor
Accelerometer

Development of non-destructive tools for determining mango ripeness would improve the quality of industrial production of the postharvest processes. This study addresses the creation of a new sensor that combines the capability of obtaining mechanical and optical properties of the fruit simultaneously. It has been integrated into a robot gripper that can handle the fruit obtaining non-destructive measurements of firmness, incorporating two spectrometer probes to simultaneously obtain reflectance properties in the visible and near-infrared, and two accelerometers attached to the rear side of two fingers. Partial least square regression was applied to different combinations of the spectral data obtained from the different sensors to determine the combination that provides the best results. Best prediction of ripening index was achieved using both spectral measurements and two finger accelerometer signals, with $R^2_P = 0.832$ and RMSEP of 0.520. These results demonstrate that simultaneous measurement and analysis of the data fusion set improve the robot gripper features, allowing assessment of the quality of the mangoes during pick and place operations.

* Corresponding author.
E-mail address: pautalens@tal.upv.es (P. Talens).

http://dx.doi.org/10.1016/j.biosystemseng.2017.08.005

1. Introduction

Mango (*Mangifera indica* L.) is a tropical fruit marketed throughout the world with a very high economic importance (Calatrava, 2014, chap. 2; Luke, 2013) and is generally harvested a little before the fully mature stage to avoid the onset of climacteric respiration during transportation to distant markets (Jha, Chopra, & Kingsly, 2007). Therefore, mango requires a ripening period before it achieves the taste and texture desired at the time of consumption (Cortés et al., 2016). The ripening process, and hence the organoleptic quality, is regulated by genetic and biochemical events that result in biochemical changes such as the biosynthesis of carotenoids (Mercadante & Rodriguez-Amaya, 1998), loss of ascorbic acid (Hernández, Lobo, & González, 2006), increase in total soluble solids (Padda, do Amarante, Garcia, Slaughter, & Mitcham, 2011), physical changes in mass, size, shape, firmness and colour etc. (Kienzle et al., 2011; Ornelas-Paz, Yahia, & Gardea-Bejar, 2008), and changes in aroma, nutritional content and flavour of the fruit (Giovannoni, 2004). The evaluation of these changes plays an important role for determining the ripening level at harvest, which will decide the market (i.e. domestic, export) and/or price of the product. Traditional determination of these changes has required a destructive methodology using specialised equipment, procedures and trained personnel, which results in high analysis costs (Torres, Montes, Perez, & Andrade, 2013). In addition, destructive methods allow only a small set of samples to be analysed to represent the variability of the whole production, though the ideal situation could be only achieved if all fruits are inspected in automated lines (Kondo, 2010). Traditionally, electronic sorters based on computer vision, used in postharvest to inspect the quality of the fruit, work at a very high speed, analysing the surface of the fruits but not providing any internal inspection. The most advanced and innovative sorters can incorporate NIR technology for testing the internal properties of produce, e.g. Vélez-Rivera, Gómez-Sanchis, et al. (2014) and Vélez-Rivera, Blasco, et al. (2014) developed computer vision techniques to determine damages and ripeness of mango 'Manila' through colour measurements. However light is projected on to the fruit from a fixed distance and the reflected or transmitted light is also measured at a certain fixed distance from the fruit. As the fruits have different sizes and shapes, the measurements can be strongly influenced by these features.

Robots have enormous potential to automate production in the food sector (Blasco, Aleixos, & Moltó, 2003; Wilson, 2010). Their main current function is to transport and manipulate objects but they have clear difficulties when handling soft and variable products (Bogue, 2009). Advances in new robot grippers are allowing their introduction in industrial and manufacturing systems for monitoring and controlling production (Tai, El-Sayed, Shahriari, Biglarbegian, & Mahmud, 2016). Automation with robots, in primary packaging operations, makes it possible to incorporate different sensors that can be used to assess fruit quality. Tactile sensors added to gripper fingers provide the capability to evaluate a product through physical contact (Lee & Nicholls, 1999) and have been used for classifying aubergine (Blanes, Ortiz, Mellado, & Beltrán, 2015) and to assess the firmness of mangoes cv. 'Osteen' (Blanes, Cortés, Ortiz, Mellado, & Talens, 2015) with a good prediction performance of the PLS model ($R^2_P = 0.760$ and RMSEP = 17.989).

Visible and near-infrared spectroscopy combined with multivariate analysis has been widely used for quantitative determination of several internal properties or compounds, to determine ripeness and to measure quality indices in fruits in general and in mango in particular (Cortés et al., 2016; Jha et al., 2013; Schmilovitch, Mizrach, Hoffman, Egozi, & Fuchs, 2000; Theanjumpol, Self, Rittiron, Pankasemsu, & Sardsud, 2013). Cortés et al. (2016) predicted, in a laboratory study, the internal quality index for cv. 'Osteen' mangoes using visible and near-infrared spectrometry (VIS–NIR), obtaining good results with the full spectral range and some selected wavelengths ($R^2_P = 0.833$ and $R^2_P = 0.815$, respectively). Thus, incorporating the capability of performing spectral measurements into gripper fingers in combination with other sensors would multiply the possibilities of measuring internal fruit quality when the fruit is handled. However, this would require development of sensor fusion techniques to obtain the maximum value from the combined information of all the sensors, and avoid redundancy (Cimander, Carlsson, & Mandenius, 2002).

Furthermore, sensor fusion enables rapid and economical in-line implementation for fruit quality assessment (Ignat, Alchanatis, & Schmilovitch, 2015). Multiple sensors have been widely used in a variety of fields. Steinmetz, Roger, Moltó, & Blasco (1999) developed a robotic quality inspection system for apples that included a colour camera and NIR spectroscopy to predict sugar content using sensor fusion techniques. Since then, significant advances in the field of sensor fusion for food products have been developed, for example in computer vision and near-infrared spectroscopy to assess fish freshness (Huang et al., 2016), fusion of impedance e-tongue and optical spectroscopy to determine the botanical origin of honey (Ulloa et al., 2013), sensor fusion of electronic nose and acoustic sensor to improve mango ripeness classification (Zakaria et al., 2012) and fusion of electronic nose, near-infrared spectrometer and standard bioreactor probes to monitor yoghurt fermentation (Cimander et al., 2002). Hitherto, examples of combination of visible and near-infrared spectroscopy spectral data and tactile sensors in a robot gripper are non-existent. Therefore, getting a sensor fusion system integrating tactile and spectral properties of the fruit would be a key advance for the post-harvest industry.

Thus, the aim of this study is to develop a novel robotic gripper that incorporates accelerometers and fibre-optic probes coupled to a spectrometer to analyse mango ripening state by simultaneously measuring firmness and visible and near-infrared reflectance when the fruit is handled in the packing house during postharvest operations.

2. Materials and methods

2.1. Experimental procedure

A batch of 275 unripe mangoes (*M. indica* L., cv 'Tommy Atkins') were selected with similar size and colour and free of

external damage. During the experiments, fruits were ripened in a storage chamber at 20.0 ± 2.1 °C and 67.6 ± 3.3% RH and fruits were divided into sets of 45 fruits each (sets marked as M1, M2, M3, M4, M5 and M6). Every 2–3 days one set was analysed, starting with set M1, until the last set M6 reached senescence (18 days). All the mangoes in each set were handled by the robotic gripper to obtain non-destructive measurements and later their physicochemical properties (total soluble solids, titratable acidity and destructive firmness) were evaluated. Prior to the measurements, the temperature of the mangoes was stabilised at 24 ± 1 °C.

2.2. Reference analysis

Routine methods were used to determine the quality attributes of the mangoes. Mango firmness was measured using a Universal Testing Machine (TextureAnalyser-XT2, Stable MicroSystems (SMS), Haslemere, England) through puncture tests using a 6 mm diameter cylindrical probe (P/15ANAME-signature) until a relative deformation of 30% of fruit size, at a speed of 1 mm s^{-1}. Two measurements were performed per fruit, on opposite sides of the equator. The fracture strength (F_{max}, N) was also obtained for all samples.

The total soluble solids (TSS) content was determined by refractometry (%) with a digital refractometer (set RFM330+, VWR International Eurolab S.L Barcelona, Spain) at 20 °C with a sensitivity of ±0.1 °Brix. Samples were analysed in triplicate.

The analysis of the titratable acidity (TA) was performed with an automatic titrator (CRISON, pH-burette 24, Barcelona, Spain) with 0.5 N NaOH until a pH of 8.1 (UNE34211:1981), using 15 g of crushed mango which was diluted in 60 mL of distilled water. The TA was determined based on the percentage of citric acid that was calculated using Eq. (1).

$$\text{TA [g citric acid/100 g of sample]} = \left(\left((A \times B \times C)\cdot D^{-1}\right) \times 100\right)\cdot E^{-1} \quad (1)$$

where A is the volume of NaOH consumed in the titration (in L), B is the normality of NaOH (0.5 N), C is the molecular weight of citric acid (192.1 g mol^{-1}), D is the mass of the sample (15 g) and E is the valence of citric acid ($E = 3$).

A multi-parameter ripening index (RPI) was calculated using Eq. (2), described previously by Vásquez-Caicedo, Sruamsiri, Carle, and Neidhart (2005) and Vélez-Rivera, Blasco, et al. (2014):

$$\text{RPI} = \ln\left(100\cdot F_{max}\cdot \text{TA}\cdot \text{TSS}^{-1}\right) \quad (2)$$

where F_{max} is the fracture strength (N), TSS is the total soluble solids (g soluble solids per 100 g of sample) and TA is the titratable acidity (g citric acid equivalent per 100 g of sample). This index was then used as reference to test the measurements obtained by the robot gripper.

2.3. Robot gripper

A robot gripper has been specifically developed to handle quasi-spherical fruit and was programmed in these experiments to work with mango fruits. The gripper has four fingers: *FA1*, *FA2*, *FB1* and *FB2* (Fig. 1). The design of the gripper fingers and its mechanical configuration can adapt to a wide range of varied shapes during handling, and provides a good performance of the accelerometers as intrinsic tactile sensors (Blanes, Mellado, & Beltrán, 2016). The *FA2*, which has a hemispherical concave shape, is attached to the chassis of the gripper and linked by a ball joint. The *FA1* is linked to a pneumatic cylinder (DSN 10-80P, Festo, Germany) with a float joint and has straight motion aligned with *FA2*. The *FB1* and *FB2* are linked to their respective pneumatic cylinders (CD85N10-50B, SMC, Japan) with two float joints and move on parallel paths. *FA1*, *FB1* and *FB2* have pads of a latex membrane filled with sesame seeds. Each pad is soft when its internal pressure is atmospheric or slightly higher and hard when its internal pressure is lower than atmospheric. The design of these fingers allows the gripper to adapt to every mango shape while it is grasped. The gripper was attached to a delta robot (IRB 340, Flexpicker, ABB, Switzerland).

In addition, the gripper was equipped with two types of sensors, two accelerometers (*ACC1* and *ACC2*) and two reflectance probes (*P1* and *P2*). The signals captured by the sensors were recorded in a laptop by means of a data acquisition module (USB 6210, National Instruments, USA) in the

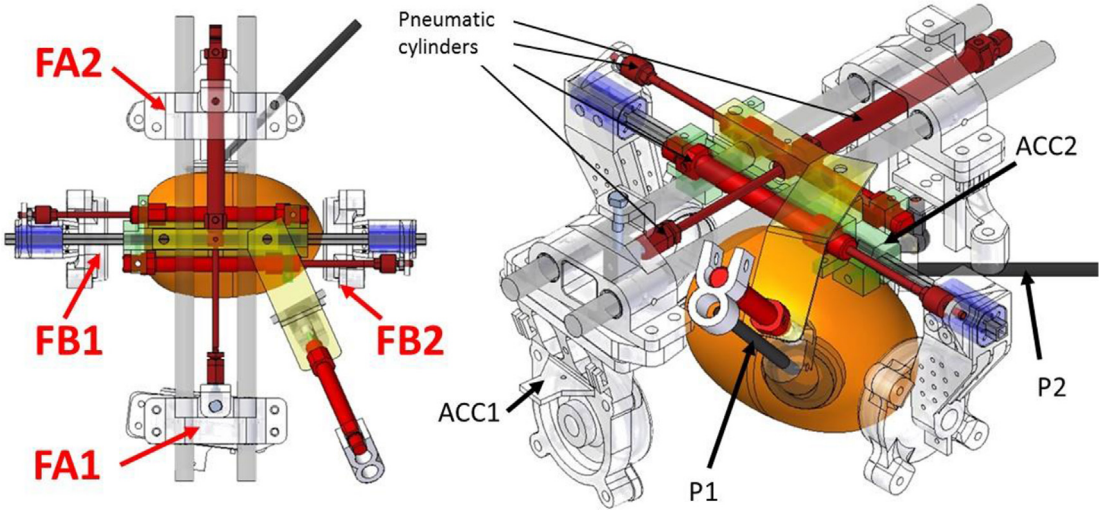

Fig. 1 – Robot gripper with the accelerometers (ACC1 and ACC2) and the VIS–NIR spectrometer probes (P1 and P2).

case of accelerometers, and a multichannel VIS–NIR spectrometer platform (AVS-DESKTOP-USB2, Avantes BV, The Netherlands) for the reflectance probes (Fig. 2).

Accelerometers *ACC1* and *ACC2* were joined to the rear side of the *FA1* and *FA2* respectively. They are intrinsic tactile sensors because they are not in direct contact to every manipulated mango. *P2* was attached to the *FA2* through a hole made in this finger. It was able to collect data as soon as both *FA1* and *FA2* were closed. Once *FA1* and *FA2* grasp a mango, *P1* approximates by means of the pneumatic cylinder action (C85E10-40, SMC, Japan). This probe was linked to the pneumatic cylinder rod by means of a ball joint. Ball joints allowed the probes to adapt to the shape of every different mango since they can rotate freely around three rotation axes.

Due to the mechanical configuration of the gripper, the sensors took measurements at different points over the surface of every mango (Fig. 3).

2.3.1. *VIS–NIR reflectance signals*

Each reflectance probe, consisting of seven fibres with a diameter of 200 μm, delivered light to the sample through a bundle of six fibres, and collected the reflected light through the seventh one. The probe tip was designed to provide reflectance measurements at an angle of 45° so as to avoid specular reflectance from the surface of the fruit.

The spectra of mango samples were collected in reflectance mode using the multichannel spectrometer platform equipped with two detectors and a quartz beam splitter (BSC-DA, Avantes BV, The Netherlands). The first detector (AvaSpec-ULS2048 StarLine, Avantes BV, The Netherlands) included a 2048-pixel charge-coupled device (CCD) sensor (SONY ILX554, SONY Corp., Japan), 50 μm entrance slit and a 600 lines mm^{-1} diffraction grating covering the working visible and near-infrared (VNIR) range from 600 nm to 1100 nm with a spectral FWHM (full width at half maximum) resolution of 1.15 nm. The spectral sampling interval was 0.255 nm. The second detector (AvaSpec-NIR256–1.7 NIRLine, Avantes BV, The Netherlands) was equipped with a 256 pixel non-cooled InGaAs (Indium Gallium Arsenide) sensor (Hamamatsu 92xx, Hamamatsu Photonics K.K., Japan), a 100 μm entrance slit and a 200 lines mm^{-1} diffraction grating covering the working NIR range from 900 nm to 1750 nm and a spectral FWHM resolution of 12 nm. The spectral sampling interval was 3.535 nm. Two Y-shaped fibre-optic reflectance probes (*P1* and *P2*) (FCR-7IR200-2-45-ME, Avantes BV, The Netherlands) were configured each with an illumination leg which connects the fibre-optic probe to stabilised 10 W tungsten halogen light sources (AvaLight-HAL-S, Avantes BV, The Netherlands). The light sources ensure a permanent light intensity over the whole measurement range. The other leg of the Y-fibre-optic probe was connected to a beam combiner (BSC-DA, Avantes BV, The Netherlands) which converted the two light beams into one light beam. Only this light beam was transmitted through another Y-shaped fibre-optic probe to both detectors for simultaneous measurement.

The calibration was performed using a 99% reflective white reference tile (WS-2, Avantes BV, The Netherlands) so that the

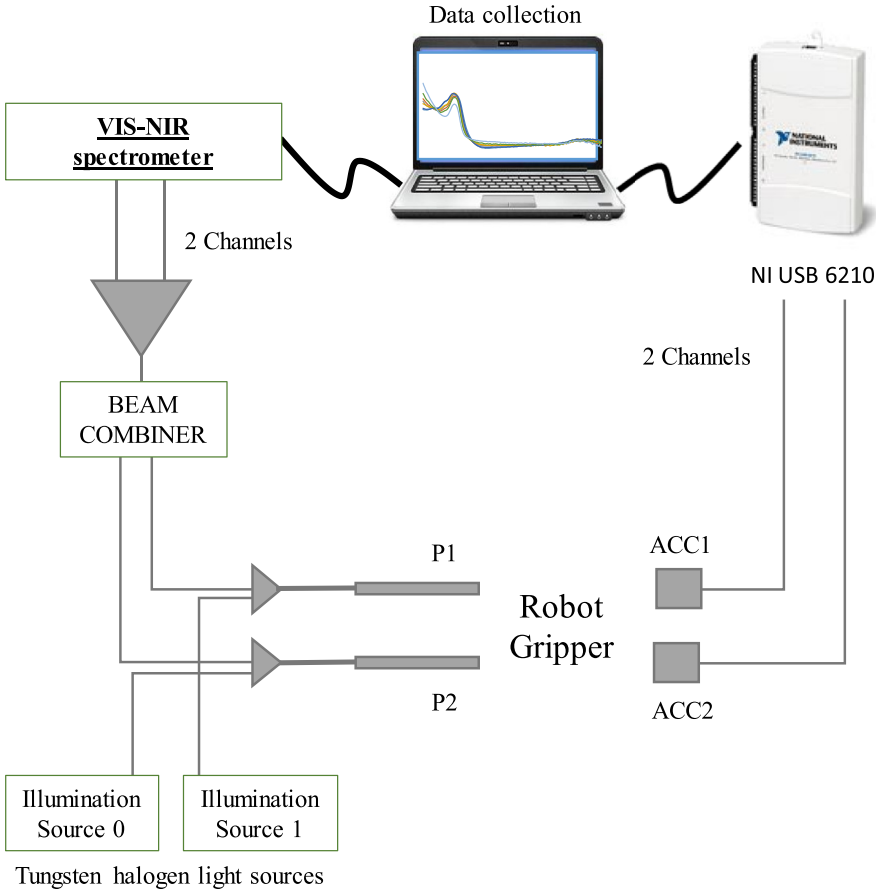

Fig. 2 – Diagram of the robot gripper, the sensors and the devices used to connect the sensors to the laptop.

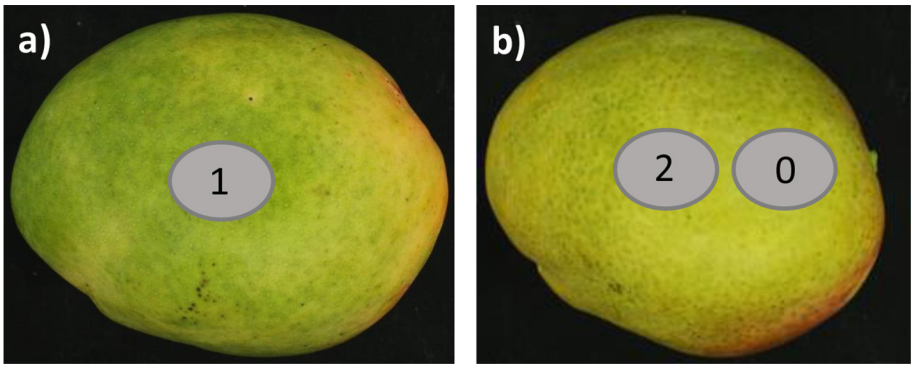

Fig. 3 – Non-destructive measurements in fruit by sensor fusion side view a) and b) (0: acquisition point of VIS–NIR spectrum with P1; 1: acquisition point of VIS–NIR spectrum with P2 and the accelerometer ACC2; 2: acquisition point of the accelerometer ACC1.

maximum reflectance value over the range of wavelengths was around 90% of saturation. The integration time was set to 240 ms for the VNIR detector and to 4200 ms for the NIR detector due the different features of both detectors. For both detectors, each spectrum was obtained as the average of five scans to reduce the thermal noise of the detector (Nicolaï et al., 2007). The average reflectance measurements of each sample (*S*) were then converted into relative reflectance values (*R*) with respect to the white reference using dark reflectance values (*D*) and the reflectance values of the white reference (*W*), as shown in Eq. (3):

$$R = \frac{S - D}{W - D} \tag{3}$$

The dark spectrum was obtained by turning off the light source and completely covering the tip of the reflectance probe.

2.3.2. *Accelerometer signals*

The accelerometers used (ADXL278, Analog Devices, USA) have a measurement range of ±50 g. They are capable of sensing collisions and, motoring and control vibration. Only the deceleration signals of the axes normal to the fingers were collected. They were sampled during approximately 0.27 s at 30 kHz and low-pass filtered (Fig. 4a), but only less than 0.1 s of signal was used for analysing the tactile sensor responses. These signals were only processed between t_0 (0.0366 s) and t_1 (0.08 s) (Fig. 4b) to capture the first contacts of the gripper fingers with every mango. Signals were rearranged using the maximum values as reference, for in this way maximum values will always be at 0.0125 s. Signals were also cut to collect 0.0315 s (Fig. 4c) and were transformed by Fast Fourier Transform using LabVIEW 11.0 (National Instruments, USA), using the option measurement magnitude root main square with Hanning window, in order to obtain the frequency distribution of energy (Fig. 4d).

2.4. *Robot gripper process and signal acquisition*

A robot program controls every grasping and sensing operation of the gripper. Three electrovalves (SY3120, SMC, Japan) were used, one for the motion of *FA1*, one the motion of *FB1* and *FB2* and the last for moving the *P2*. Two adjustable flowmeter control valves (AS2201F-01-04S, SMC, Japan) were used to adjust the speed of *FA1* and *P2*. A vacuum generator with blow function (VN-07-H-T3-PQ2-VQ2-RO1-B, Festo, Germany) provides the possibility of controlling the hardness of *FA1* by means of its internal valves 2 and 4. The data acquisition device used to collect the accelerometer signals starts to collect data when the robot sends the signal to close *FA1*.

When the gripper is at the approach position to grasp a mango, valve 1 is activated for closing *FA1*. After 0.3 s, valve 2 is activated for 0.05 s to change the pad of *FA1* to a softer state. During this time, valve 1 is deactivated to open *FA1*. Then, the signals of the valves 1 and 3 are activated to close *FA1*, *FB1* and *FB2* during 0.3 s and the pad of *FA1* changes to a harder state (valve 4 activated) and waits for 0.5 s. This process adapts the pad of *FA1* to every mango shape. The *P2* starts to collect data. The robot moves the gripper up. The pad of the *FA1* is in the hard state and starts an open/close loop (open during 0.05 s, close for 1 s). During this loop, the signals of *ACC1* and *ACC2* are collected. Then, valve 5 is activated, *P1* approaches the mango surface and starts to collect data. The whole process is shown in Fig. 5.

2.5. *Signal pre-processing and statistical analysis*

The raw spectra from the spectrometer were transformed to apparent absorbance (log(1/R)) values using The Unscrambler Version 10.2 software package (CAMO Software AS, Oslo, Norway) to obtain linear correlations of the NIR values with the concentration of the estimated constituents (Liu, Jiang, & He, 2009; Shao et al., 2007) and centred by subtracting their averages in order to ensure that all results will be interpretable in terms of variation around the mean.

Figure 6 shows raw VNIR and NIR spectra and its correction after the application of the pre-processing methods. Savitzky–Golay smoothing (with segment size 15) was applied to improve the signal-to-noise ratio in order to reduce the effects caused by the physiological variability of samples (Beghi, Giovenzana, Brancadoro, & Guidetti, 2017; Carr, Chubar, & Dumas, 2005). Due to the fresh fruit light scattering (Santos, Trujillo, Calero, Alfaro, & Muñoz, 2013), the light does not always travel the same distance into the sample before it is

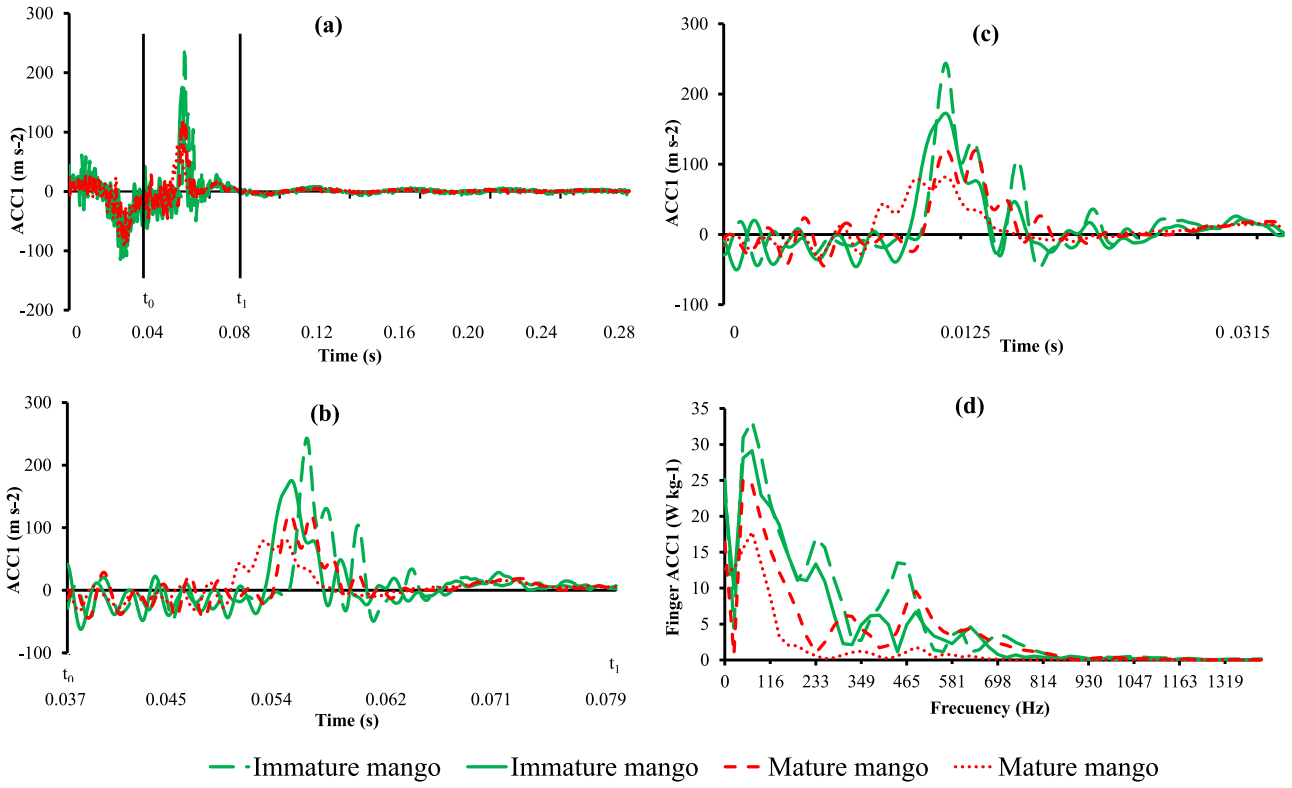

Fig. 4 – An example of the process done for processing deceleration signals as tactile sensors. (a) Original collected signals for decelerations of FA1 for mangoes with different ripeness state, (b) cut signal between t_0 and t_1 and (c) signals reordered around the maximum values and (d) the spectra of the signals.

detected. A longer light travelling path corresponds to a lower relative reflectance value, since more light is absorbed. This causes a parallel translation of the spectra. This kind of variation is not useful for the calibration models and needs to be eliminated by the EMSC technique (Bruun, Sondergaard, & Jacobsen, 2007; He, Li, & Deng, 2007; Martens, Nielsen, & Engelsen, 2003). In addition to these pre-processing steps, the second derivate with Gap-Segment (2.3) gave the best results for the NIR spectra because it allowed the extraction of useful information (Rodriguez-Saona, Fry, McLaughlin, & Calvey, 2001). The different pre-treatments were applied in the sequence explained, specifying that the first two pre-treatments (smoothing and EMSC) were only applied to the VNIR spectra and those two with the third (second derivate) applied to the NIR spectra (Cortés et al., 2016). Finally, the adjustment to the spectral intensities from each sensor ACC1, ACC2, P1 and P2 was range-normalised so the data from all samples were directly comparable to each other (Andrés & Bona, 2005; Blanco, Alcalá, González, & Torras, 2006).

The different sensor signals were combined through a 'low-level' fusion procedure (Roussel, Bellon-Maurel, Roger, & Grenier, 2003a,b) by concatenating the pre-processed sensor signals – appending one to another – to create a single matrix with a total of 5516 variables, which was processed using The Unscrambler. Data were organised in a matrix where the rows represent the number of samples (#N = 275 samples) and the columns represent the variables (X-variables and Y-variables). The X-variables, or predictors, were the signals obtained by fusion of the data from the two fibre-optic probes of the spectrometer and the accelerometers. The Y-variable, or response, was the RPI of each sample. In order to correct the relative influences of the different instrumental responses on the model, a standardisation technique was used, where the weight of each X-variable was the standard deviation of the variable (Bouveresse, Hartmann, Last, Prebble, & Massart, 1996). Then, fifteen regression models for each combination of the spectra data from the different sensors were developed by partial least squares (PLS) to predict RPI. Samples were randomly separated into two groups, and 75% of the samples were used to develop the model that was validated by cross validation, while the remaining samples (25%) were used as the prediction set. The root mean square error of calibration (RMSEC), root mean squared error of cross validation (RMSECV), the root mean square error of prediction (RMSEP), the coefficient of determination for calibration (R^2_C), for prediction (R^2_P) and for cross validation (R^2_{CV}), and the required number of latent variables (LV) were used to judge the accuracy of the PLS model.

3. Results and discussion

3.1. *Changes in mango quality during ripening*

The changes observed in the physicochemical characteristics (F_{max}, TSS and TA) of mangoes during postharvest storage are shown in Table 1.

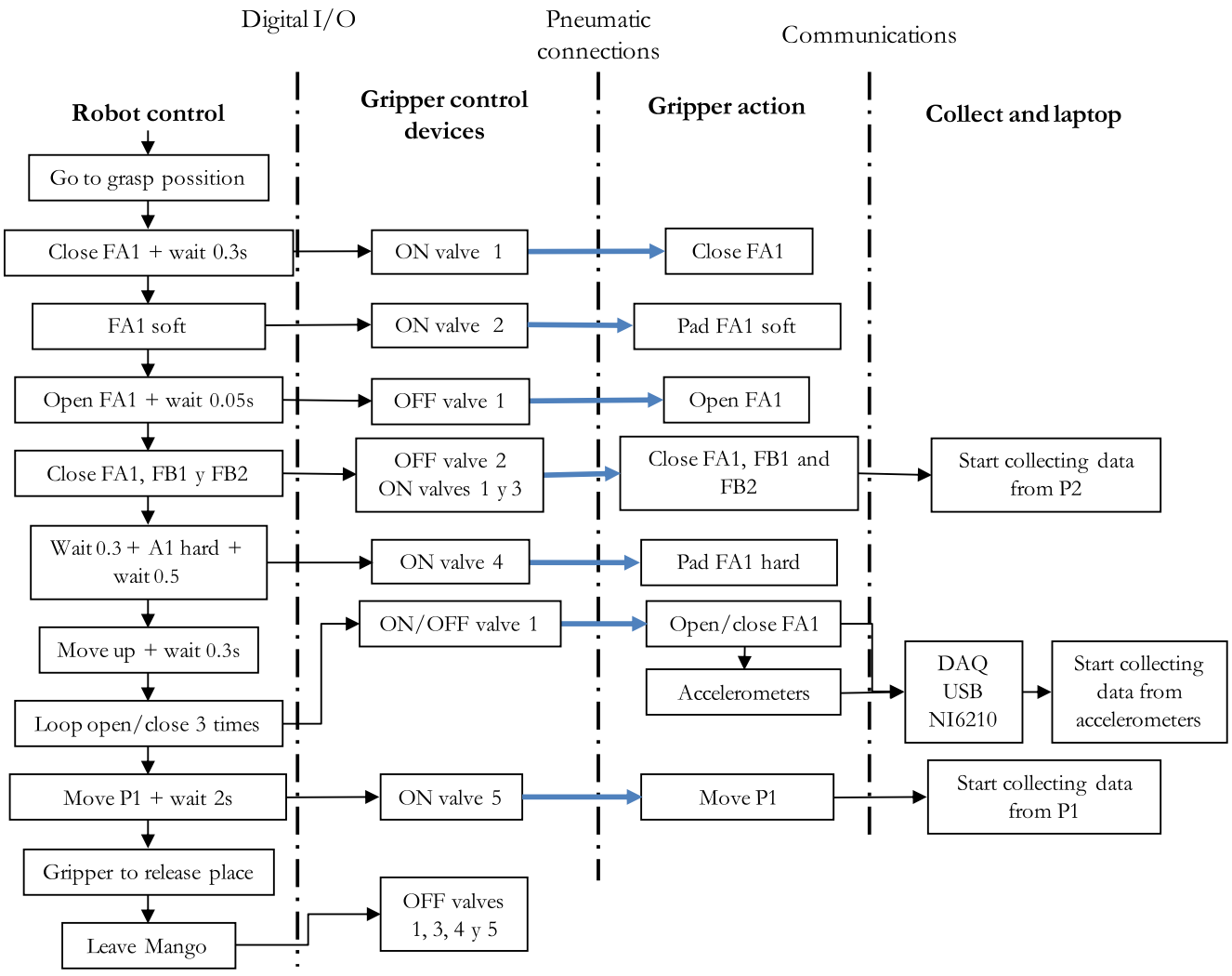

Fig. 5 – Diagram of the robot control operation the signals over gripper control devices, the gripper action and the collecting data of the sensors.

For all sets of mangoes there was a steady decrease in fruit firmness over time starting around 137 N and falling to 28 N. These changes are due to significant changes in the composition and structure of cell walls and middle lamellae due to the solubilisation, de-esterification and de-polymerisation of the middle lamella (Singh, Singh, Sane, & Nath, 2013), and the enzymatic activity (Prasanna, Prabha, & Tharanathan, 2007; Yashoda, Prabha, & Tharanathan, 2007). A similar behaviour has been reported for other mango varieties such as 'Alphonso' (Yashoda, Prabha, & Tharanathan, 2005), 'Ataulfo' (Palafox-Carlos et al., 2012), 'Keitt' (Ibarra-Garza, Ramos-Parra, Hernández-Brenes, & Jacobo-Velázquez, 2015) and 'Osteen' (Cortés et al., 2016). Similarly, TA tends to decrease due to cell metabolisation of volatile organic acids and non-volatile constituents (Padda et al., 2011), and in addition acids can be used as substrates for respiration when sugars have been consumed or have participated in the synthesis of phenolic compounds, lipids and volatile aromas (Abu-Goukh, Shattir, & Mahdi, 2010). In contrast, the TSS increased continuously during postharvest storage due to the conversion of starch to glucose and fructose, which are used as substrates during fruit respiration (Eskin, Hoehn, & Shahidi, 2013). Similar results have been observed by Quintana, Nanthachai, Hiranpradit, Mendoza, and Ketsa (1984), who reported that TSS of mango increased gradually up to full ripeness.

RPI was calculated for every day of storage. Figure 7 shows the evolution of the RPI through median plots with 95% confidence intervals during storage. The values of the index clearly decreased during ripening. Initially, the RPI declined sharply as the fruits ripen to achieve their optimum organoleptic properties, and then the fruit reached the stage of over-ripeness where the curve follows a constant trend because the product reaches a maximum content of TSS and minimum firmness and TA.

3.2. *Non-destructive prediction of mango ripening*

The data were concatenated (accelerometers and VIS–NIR spectra) (Decruyenaere et al., 2009; Roussel et al., 2003a,b) to

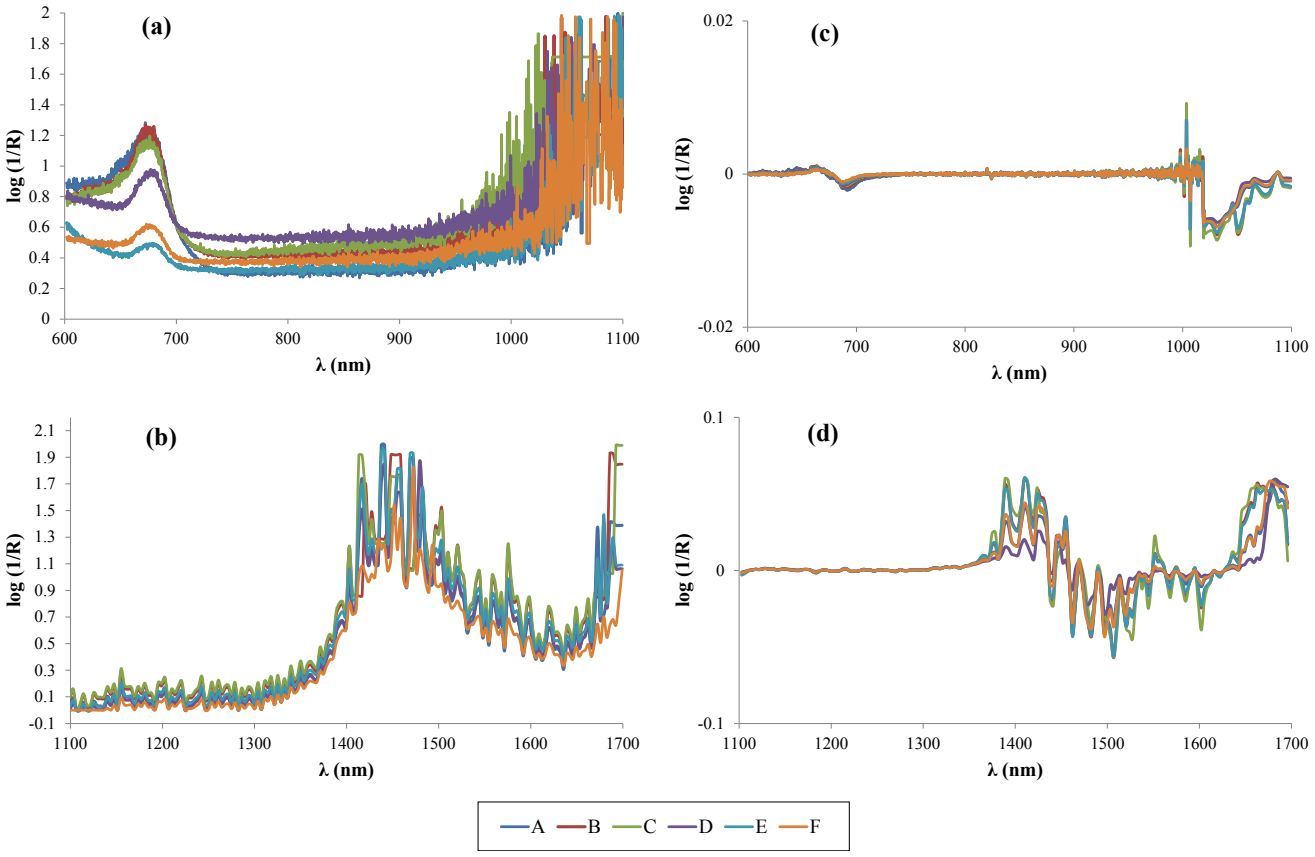

Fig. 6 – Averaged raw spectra (left) and averaged final spectra obtained with the pre-treatment and transformed signals (right) of the each set for (a,c) the VNIR region; and (b,d) the NIR region.

Table 1 – Descriptive statistics for the quality parameters analysed in mango samples during the storage period.

		Set A	Set B	Set C	Set D	Set E	Set F
Mechanical properties	F_{max} (N)	137 ± 18a	62 ± 16b	45 ± 16c	34 ± 11d	35 ± 8d	28 ± 8e
Internal composition	TSS (%)	10.4 ± 0.9a	12 ± 1b,c	12 ± 1c,d	12 ± 1d	12 ± 1b	12 ± 2b,c
	TA (%)	0.8 ± 0.2a	0.62 ± 0.15b	0.41 ± 0.08c	0.30 ± 0.06d	0.29 ± 0.06d	0.19 ± 0.05e

Values are mean ± SD.
a–e Different letters in the same row indicate significant difference among sets ($p < 0.05$).

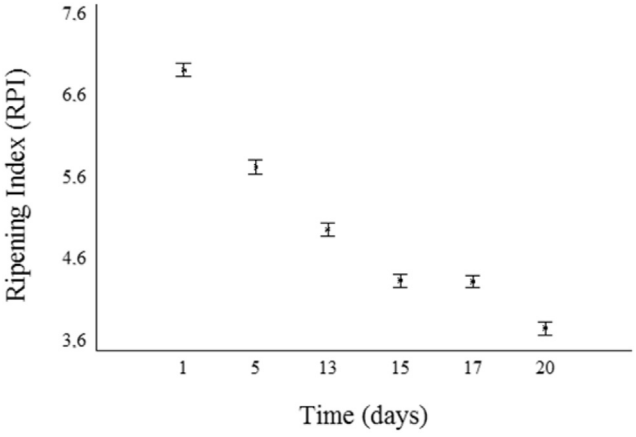

Fig. 7 – Evolution of the RPI during storage period of the mango samples.

form a representative complex spectrum with a total of 5516 variables. Table 2 shows the results of the validation and prediction results of the PLS models built for the data obtained by every single sensor and for the data fusion (due to the concatenation of wavenumber) performed among all possible combinations of spectral data.

The best PLS model for prediction of RPI is presented in Fig. 8. Figure 9 shows the regression coefficients of the best developed model and the PRESS plot for identifying the optimum number of LVs. The results for this model were obtained using VIS–NIR fibre-optic probes and the two accelerometer signals. The calibration model for predicting RPI has an $R^2_C = 0.945$ and RMSEC = 0.235, and the validation of the calibration model has an $R^2_{CV} = 0.804$ and RMSECV = 0.447. The prediction model indicates a good prediction performance, with $R^2_P = 0.832$ and RMSEP = 0.520.

Table 2 – Comparison of the prediction of mango ripening provided by different possible combination of sensor fusion to the two fibre-optic probes of VIS–NIR spectrometer and two accelerometers located at the fingers of the robot gripper.

Sensors	#LV	Calibration set				Prediction set	
		R^2_C	RMSEC	R^2_{CV}	RMECV	R^2_P	RMSEP
P2	1	0.769	0.506	0.742	0.537	0.732	0.663
P1	3	0.895	0.323	0.739	0.512	0.632	0.727
P2 + P1	3	0.933	0.268	0.782	0.487	0.802	0.554
ACC1	6	0.677	0.574	0.575	0.663	0.444	0.871
ACC2	4	0.611	0.626	0.48	0.727	0.300	1.020
ACC1 + ACC2	4	0.758	0.758	0.595	0.595	0.655	0.737
P2 + ACC1	2	0.854	0.373	0.77	0.471	0.778	0.613
P2 + ACC2	1	0.695	0.586	0.649	0.632	0.733	0.665
P1 + ACC1	4	0.940	0.251	0.753	0.513	0.662	0.698
P1 + ACC2	5	0.971	0.175	0.776	0.493	0.662	0.742
P2 + P1 + ACC1	4	0.973	0.166	0.786	0.467	0.797	0.550
P2 + P1 + ACC2	2	0.867	0.379	0.777	0.494	0.784	0.595
P2 + ACC1 + ACC2	2	0.813	0.460	0.705	0.580	0.813	0.567
P1 + ACC1 + ACC2	5	0.971	0.176	0.779	0.490	0.733	0.642
P2 + P1 + ACC1 + ACC2	3	0.945	0.235	0.804	0.447	**0.832**	0.520

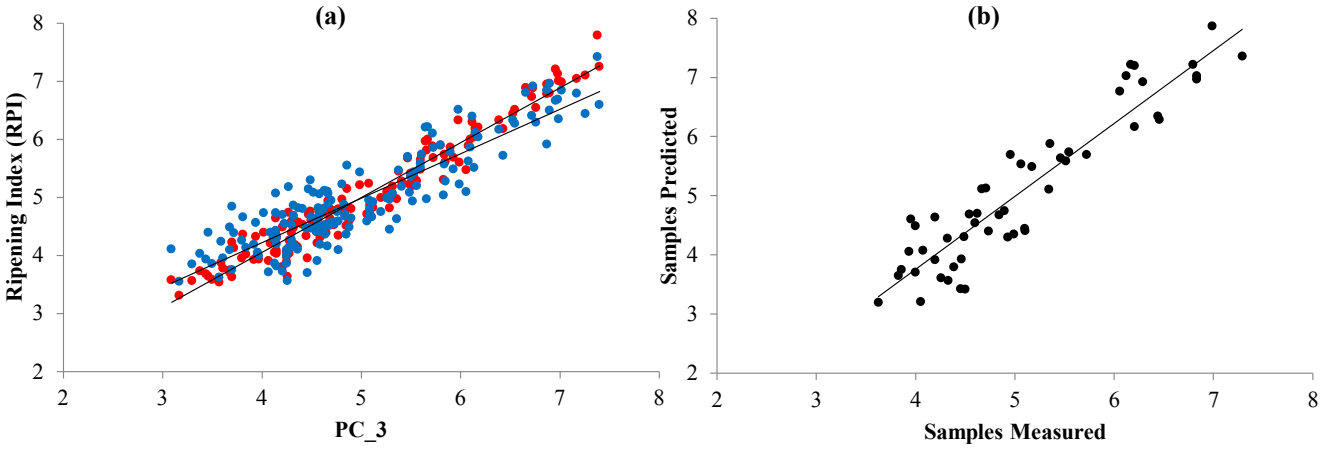

Fig. 8 – Performance of the PLS model (a) cross validation, respectively: calibration samples (blue) and validation samples (red), and (b) prediction of the RPI in mango cv. 'Tommy Atkins', built using the data from all the probes and accelerometers four sensors which resulted the best combination.

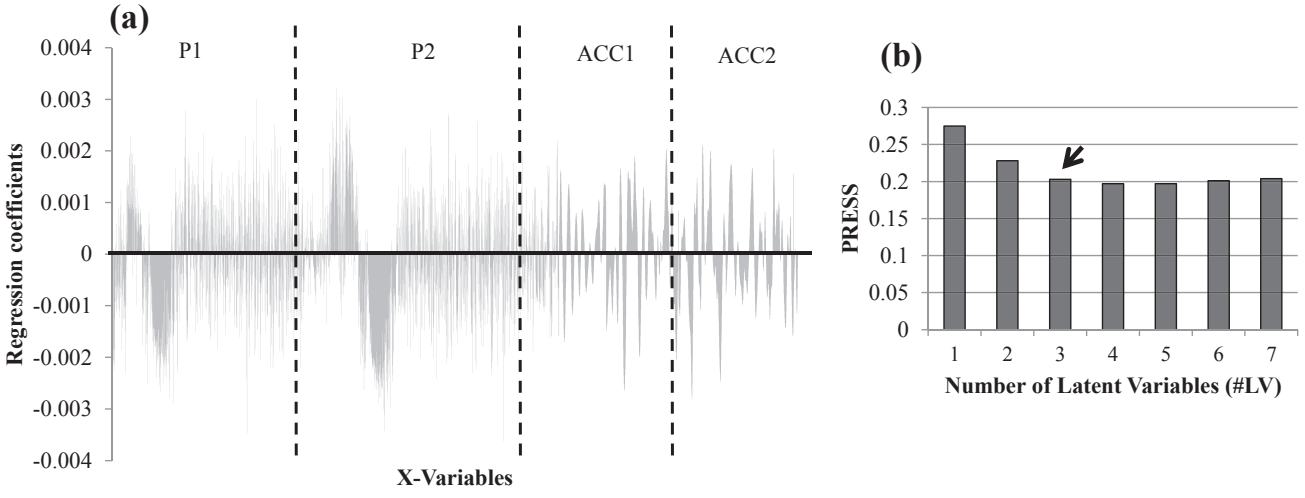

Fig. 9 – (a) Regression coefficients of three-components PLS model containing the fused individual matrices of the calibration set as *X*-variables and the RPI as the *Y*-variables. (b) The number of latent variables of the same model.

3.3. *Integration of tactile sensing and reflectance data in the robot gripper*

This novel gripper presents an important evolution from previous grippers for sensing and handling the firmness of aubergines and mangoes by using accelerometers as tactile sensors (Blanes, Ortiz, et al., 2015; Blanes, Cortés, et al., 2015). Unlike these previous grippers, which caused damage in some over-ripe mangoes due to the action of a suction cup needed for holding the fruits, this new gripper incorporates four fingers and intrinsic sensors that avoid the need of a suction cup when holding the fruit for measurement and placing.

Besides, the combination of the two probes achieved better results than *P2* or *P1* standalone, having an R^2_P of 0.802 compared to 0.732 and 0.632, respectively. In the same way, *ACC1* together with *ACC2* gave a better result than *ACC1* or *ACC2* alone with an R^2_P of 0.655 compared to 0.444 and 0.300, respectively. It is important to remark that the composition of a fruit is not uniform and hence some parts of the mango may have different ripeness than others. Therefore, it is necessary to take simultaneous measurements at least for the three points studied to obtain reliable and robust results. Blanes, Cortés, et al. (2015) developed a gripper with three accelerometers to estimate the ripeness of mangoes cv. 'Osteen', achieving a $R^2_P = 0.760$ which is lower than the current robot gripper ($R^2_P = 0.832$). This highlights the important contribution of the integration of both tactile sensors and VNIR reflectance measurements in the robotic gripper to assess the quality of the mangoes during fruit handling.

A handicap of this system in the current version is the long time needed to process every mango. The incorporation of two spectrometer probes increases the processing time of every mango up to 9 s. However, experiments have been done in a first prototype for testing, where the algorithms, hardware and processes were not optimised for working at high speed. With improved integration of the hardware, optimising algorithms and parallelising some processes, the whole process could experience a dramatic reduction of the operation time. On the other hand, the combination of sensors of different nature provides the capability of obtaining simultaneously both mechanical and optical properties of the fruit. This innovative approach is highly interesting in the emerging competitive food sector where monitoring of product quality, reproducibility and traceability is decisive in manufacturing (Kondo, 2010).

4. Conclusions

A novel robot gripper equipped with sensors, i.e. with two accelerometers and two VIS–NIR reflectance probes, has been developed and tested for fruit handling. The design uses sensors that do not need direct contact, are intrinsic tactile sensors, and can take the measurements simultaneously during the mango handling, which is an important advantage over the state of the art. The results show good prediction of the quality of the fruit, using a ripening index based on the information from VIS–NIR spectra and non-destructive impact measured during handling, achieving an R^2_P of 0.832 and RMSEP of 0.520. This innovative prototype integrates sensors of different nature, whose data information is combined to obtain better prediction. The fusion of different types of sensors like spectrometry (electromagnetic) and accelerometers (vibrational) achieved better results than using only the accelerometers, or similar results to using spectroscopy, but in this case, the measurements were made while the fruit was handled. In this way, results show the potential and advantages of performing simultaneous operations with sensors of different nature integrated on a robot gripper that can inspect and classify the mangoes by their ripeness during a pick and place robot process.

Acknowledgements

This work has been partially funded by the Instituto Nacional de Investigación y Tecnología Agraria y Alimentaria de España (INIA) and FEDER through research projects RTA2012-00062-C04-01, RTA2012-00062-C04-02, RTA2012-00062-C04-03, and by the Conselleria d' Educació, Investigació, Cultura i Esport, Generalitat Valenciana, through the project AICO/2015/122. V. Cortés thanks the Spanish MEC for the FPU grant (FPU13/04202).

REFERENCES

Abu-Goukh, A. A., Shattir, A. E., & Mahdi, F. M. (2010). Physico-chemical changes during growth and development of papaya fruit. II: Chemical changes. *Agriculture and Biology Journal of North America*, 2151–7517.

Andrés, J. M., & Bona, M. T. (2005). Analysis of coal by diffuse reflectance near-infrared spectroscopy. *Analytica Chimica Acta*, 535, 123–132.

Beghi, R., Giovenzana, V., Brancadoro, L., & Guidetti, R. (2017). Rapid evaluation of grape phytosanitary status directly at the check point station entering the winery by using visible/near infrared spectroscopy. *Journal of Food Engineering*, 204, 46–54.

Blanco, M., Alcalá, M., González, J. M., & Torras, E. (2006). Near infrared spectroscopy in the study of polymorphic transformations. *Analytica Chimica Acta*, 567, 262–268.

Blanes, C., Cortés, V., Ortiz, C., Mellado, M., & Talens, P. (2015). Non-destructive assessment of mango firmness and ripeness using a robotic gripper. *Food and Bioprocess Technology*, 8, 1914–1924.

Blanes, C., Mellado, M., & Beltrán, P. (2016). Tactile sensing with accelerometers in prehensile grippers for robots. *Mechatronics*, 33, 1–12.

Blanes, C., Ortiz, C., Mellado, M., & Beltrán, P. (2015). Assessment of eggplant firmness with accelerometers on a pneumatic robot gripper. *Computers and Electronics in Agriculture*, 113, 44–50.

Blasco, J., Aleixos, N., & Moltó, E. (2003). Machine vision system for automatic quality grading of fruit. *Biosystems Engineering*, 85, 415–423.

Bogue, R. (2009). The role of robots in the food industry: A review. *Industrial Robot: An International Journal*, 36(6), 531–536.

Bouveresse, E., Hartmann, C., Last, I. R., Prebble, K. A., & Massart, L. (1996). Standardization of near-infrared spectrometric instruments. *Analytical Chemistry*, 68, 982–990.

Bruun, S. W., Sondergaard, I., & Jacobsen, S. (2007). Analysis of protein structures and interactions in complex food by near-

infrared spectroscopy. 1. Gluten powder. *Journal of Agricultural and Food Chemistry, 55*, 7234–7243.
Calatrava, J. (2014). Mango, economics and international trade. In *Mango international encyclopedia*. Sultanate of Oman: Royal Court Affairs Ed.
Carr, G. L., Chubar, O., & Dumas, P. (2005). In R. Bhargava, & I. W. Levin (Eds.), *Spectrochemical analysis using infrared multichannel detectors* (1st ed., pp. 56–84). Oxford: Wiley-Blackwell.
Cimander, C., Carlsson, M., & Mandenius, C. F. (2002). Sensor fusion for on-line monitoring of yoghurt fermentation. *Journal of Biotechnology, 99*, 237–248.
Cortés, V., Ortiz, C., Aleixos, N., Blasco, J., Cubero, S., & Talens, P. (2016). A new internal quality index for mango and its prediction by external visible and near-infrared reflection spectroscopy. *Postharvest Biology and Technology, 118*, 148–158.
Decruyenaere, V., Lecome, Ph, Demarquilly, C., Aufrere, J., Dardenne, P., Stilmant, D., et al. (2009). Evaluation of green forage intake and digestibility in ruminants using near infrared reflectance spectroscopy (NIRS): Developing a global calibration. *Animal Feed Science and Technology, 148*, 138–156.
Eskin, N. A. M., Hoehn, E., & Shahidi, F. (2013). Fruits and vegetables. In N. A. M. Eskin, & F. Shahidi (Eds.), *Biochemistry of foods* (pp. 49–126).
Giovannoni, J. J. (2004). Genetic regulation of fruit development and ripening. *Plant Cell, 16*, 170–180.
He, Y., Li, X., & Deng, X. (2007). Discrimination of varieties of tea using near infrared spectroscopy by principal component analysis and BP model. *Journal of Food Engineering, 79*, 1238–1242.
Hernández, Y., Lobo, M. G., & González, M. (2006). Determination of vitamin C in tropical fruits: A comparative evaluation of methods. *Food Chemistry, 96*(4), 654–664.
Huang, X., Xu, H., Wu, L., Dai, H., Yao, L., & Han, F. (2016). A data fusion detection method for fish freshness based on computer vision and near-infrared spectroscopy. *Analytical Methods, 8*, 2929–2935.
Ibarra-Garza, I. P., Ramos-Parra, P. A., Hernández-Brenes, C., & Jacobo-Velázquez, D. A. (2015). Effects of postharvest ripening on the nutraceutical and physicochemical properties of mango (*Mangifera indica* L. cv Keitt). *Postharvest Biology and Technology, 103*, 45–54.
Ignat, T., Alchanatis, V., & Schmilovitch, Z. (2015). Maturity prediction of intact bell peppers by sensor fusion. *Chemical Engineering Transactions, 44*, 67–73.
Jha, S. N., Chopra, S., & Kingsly, A. R. P. (2007). Modeling of color values for non-destructive evaluation of maturity of mango. *Journal of Food Engineering, 78*, 22–26.
Jha, S. N., Jaiswal, P., Narsaiah, K., Sharma, R., Bhardwaj, R., Gupta, M., et al. (2013). Authentication of mango varieties using near infrared spectroscopy. *Agricultural Research, 2*(3), 229–235.
Kienzle, S., Sruamsiri, P., Carle, R., Sirisakulwat, S., Spreer, W., & Neidhart, S. (2011). Harvest maturity specification for mango fruit (*Mangifera indica* L. 'Chok Anan') in regard to long supply chains. *Postharvest Biology and Technology, 61*, 41–55.
Kondo, N. (2010). Automation on fruit and vegetables grading system and food traceability. *Trends in Food Science & Technology, 21*, 145–152.
Lee, M. H., & Nicholls, H. R. (1999). Tactile sensing for mechatronics – A state of the art survey. *Mechatronics, 9*, 1–31.
Liu, F., Jiang, Y., & He, Y. (2009). Variable selection in visible/near infrared spectra for linear and nonlinear calibrations: A case study to determine soluble solids content of beer. *Analytica Chimica Acta, 635*, 45–52.
Luke, H. (2013). *'The economics of the mango trade'. Examining the economic impact of globally traded mangoes*. PDF File: University of Minnesota-Duluth Economics https://www.mcee.umn.edu/sites/mcee.umn.edu/files/heine-cloquet_high_school001-for_website.pdf.
Martens, H., Nielsen, J. P., & Engelsen, S. B. (2003). Light scattering and light absorbance separated by extended multiplicative signal correction. Application to near-infrared transmission analysis of powder mixtures. *Analytical Chemistry, 75*, 394–404.
Mercadante, A. Z., & Rodriguez-Amaya, D. B. (1998). Effects of ripening, cultivar differences, and processing on the carotenoid composition of mango. *Journal of Agricultural and Food Chemistry, 46*(1), 128–130.
Nicolaï, B. M., Beullens, K., Bobelyn, E., Peirs, A., Saeys, W., Theron, I. K., et al. (2007). Non-destructive measurement of fruit and vegetable quality by means of NIR spectroscopy: A review. *Postharvest Biology and Technology, 46*, 99–118.
Ornelas-Paz, J. D. J., Yahia, E. M., & Gardea-Bejar, A. A. (2008). Changes in external and internal color during postharvest ripening of 'Manila' and 'Ataulfo' mango fruit and relationship with carotenoid content determined by liquid chromatography–APcI+–time-of-flight mass spectrometry. *Postharvest Biology and Technology, 50*(2), 145–152.
Padda, S. M., do Amarante, C. V. T., Garcia, R. M., Slaughter, D. C., & Mitcham, E. M. (2011). Methods to analyze physicochemical changes during mango ripening: A multivariate approach. *Postharvest Biology and Technology, 62*, 267–274.
Palafox-Carlos, H., Yahia, E., Islas-Osuna, M. A., Gutierrez-Martinez, P., Robles-Sánchez, M., & González-Aguilar, G. A. (2012). Effect of ripeness stage of mango fruit (*Mangifera indica* L., cv. Ataulfo) on physiological parameters and antioxidant activity. *Scientia Horticulturae, 135*(0), 7–13.
Prasanna, V., Prabha, T. N., & Tharanathan, R. N. (2007). Fruit ripening phenomena – An overview. *Critical Reviews in Food Science and Nutrition, 47*, 1–19.
Quintana, E. G., Nanthachai, P., Hiranpradit, H., Mendoza, D. B., & Ketsa, S. (1984). Changes in mango during growth and maturation: Growth and development of mango. *ASEAN Food Handling Bureau*, 21–27.
Rodriguez-Saona, L. E., Fry, F. S., McLaughlin, A., & Calvey, E. M. (2001). Rapid analysis of sugars in fruit juices by FT-NIR spectroscopy. *Carbohydrate Research, 336*, 63–74.
Roussel, S., Bellon-Maurel, V., Roger, J. M., & Grenier, P. (2003a). Fusion of aroma, FT-IR and UV sensor data based on the Bayesian inference. Application to the discrimination of white grape varieties. *Chemometrics and Intelligent Laboratory Systems, 65*(2), 209–219.
Roussel, S., Bellon-Maurel, V., Roger, J. M., & Grenier, P. (2003b). Authenticating white grape must variety with classification models based on aroma sensors, FT-IR and UV spectrometry. *Journal of Food Engineering, 60*, 407–419.
Santos, J., Trujillo, L. A., Calero, N., Alfaro, M. C., & Muñoz, J. (2013). Physical characterization of a commercial suspoemulsion as a reference for the development of suspoemulsions. *Chemical Engineering & Technology, 11*, 1–9.
Schmilovitch, Z., Mizrach, A., Hoffman, A., Egozi, H., & Fuchs, Y. (2000). Determination of mango physiological indices by near-infrared spectrometry. *Postharvest Biology & Technology, 19*(3), 245–252.
Shao, Y., He, Y., Gómez, A. H., Pereir, A. G., Qiu, Z., & Zhang, Y. (2007). Visible/near infrared spectrometric technique for nondestructive assessment of tomato 'Heatwave' (Lycopersicumesculentum) quality characteristics. *Journal of Food Engineering, 81*(4), 672–678.
Singh, Z., Singh, R. K., Sane, V. A., & Nath, P. (2013). Mango – Postharvest biology and biotechnology. *Critical Reviews in Plant Sciences, 32*(4), 217–236.
Steinmetz, V., Roger, J. M., Moltó, E., & Blasco, J. (1999). On-line fusion of colour camera and spectrophotometer for sugar content prediction of apples. *Journal of Agricultural Engineering Research, 73*(2), 207–216.

Tai, K., El-Sayed, A. R., Shahriari, M., Biglarbegian, M., & Mahmud, S. (2016). State of the art robotic grippers and applications. *Robotics, 5*(2), 11.

Theanjumpol, P., Self, G., Rittiron, R., Pankasemsu, T., & Sardsud, V. (2013). Selecting variables for near infrared spectroscopy (NIRS) evaluation of mango fruit quality. *Journal of Agricultural Science, 5*(7), 146–159.

Torres, R., Montes, E. J., Perez, O. A., & Andrade, R. D. (2013). Relación del color y del estado de madurez con las propiedades fisicoquímicas de frutas tropicales. *Información Tecnológica, 24*(4), 51.

Ulloa, P. A., Guerra, R., Cavaco, A. M., Rosa da Costa, A. M., Figueira, A. C., & Brigas, A. F. (2013). Determination of the botanical origin of honey by sensor fusion of impedance e-tongue and optical spectroscopy. *Computers and Electronics in Agriculture, 94*, 1–11.

Vásquez-Caicedo, A. L., Sruamsiri, P., Carle, R., & Neidhart, S. (2005). Accumulation of all-trans-b-carotene and its 9-cis and 13-cis stereoisomers during postharvest ripening of nine Thai mango cultivars. *Journal of Agricultural and Food Chemistry, 53*, 4827–4835.

Vélez-Rivera, N., Blasco, J., Chanona-Pérez, J., Calderón-Domínguez, G., Perea-Flores, M. J., Arzate-Vázquez, I., et al. (2014). Computer vision system applied to classification of 'Manila' mangoes during ripening process. *Food and Bioprocess Technology, 7*, 1183–1194.

Vélez-Rivera, N., Gómez-Sanchis, J., Chanona-Pérez, J., Carrasco, J. J., Millán-Giraldo, M., Lorente, D., et al. (2014). Early detection of mechanical damage in mango using NIR hyperspectral images and machine learning. *Biosystems Engineering, 122*, 91–98.

Wilson, M. (2010). Developments in robot applications for food manufacturing. *Industrial Robot: An International Journal, 37*(6), 498–502.

Yashoda, H. M., Prabha, T. N., & Tharanathan, R. N. (2007). Mango ripening—Role of carbohydrases in tissue softening. *Food Chemistry, 102*(3), 691–698.

Yashoda, H. M., Prabha, T. N., & Tharanathan, R. N. (2005). Mango ripening—Chemical and structural characterization of pectic and hemicellulosic polysaccharides. *Carbohydrate Research, 340*(7), 1335–1342.

Zakaria, A., Shakaff, A. Y. M., Masnan, M. J., Saad, F. S. A., Adom, A. H., Ahmad, M. N., et al. (2012). Improved maturity and ripeness classifications of *Magnifera indica* cv. harumanis mangoes through sensor fusion of an electronic nose and acoustic sensor. *Sensors, 12*(5), 6023–6048.